Soft-x-ray spectra of highly charged Kr ions in an electron beam ion trap

H. Chen, P. Beiersdorfer, K. B. Fournier, and E. Träbert*
Department of Physics and Advanced Technologies, Lawrence Livermore National Laboratory, Livermore, California 94550-9234
(Received 8 October 2001; revised manuscript received 8 January 2002; published 24 April 2002)

Systematic variation of the electron-beam energy in the EBIT-II electron beam ion trap has been employed to produce soft-x-ray spectra (20–75 Å) of Kr with well-defined maximum charge states ranging from Cu- to Al-like ions. Guided by large-scale relativistic atomic structure calculations, the strongest lines have been identified with $\Delta n=1$ ($n=3$ to $n'=4$) transitions from Ni- to P-like ions (Kr^{8+}-Kr^{21+}), as well as a number of $3p$-$4d$ and $3d$-$5f$ transitions.

DOI: 10.1103/PhysRevE.65.056401 PACS number(s): 52.70.La, 32.30.Rj, 39.30.+w, 31.50.Df

I. INTRODUCTION

Fusion plasmas regularly need to be of a low effective nuclear charge Z (low impurity content in the hydrogen working gas) in order to prevent radiative losses from the central plasma. However, estimates show that the energy losses from neutral hydrogen are not enough to limit the heat load on the plasma-facing components (PFCs) in a fusion reactor to technically acceptable levels [1]. Radiation in the outermost region of the plasma from a mantle of deliberately introduced, high recycling rate impurities is seen as a possible mechanism for controlling the heat load deposited onto the PFCs of a fusion reactor [2–4]. Radiating-mantle experiments were started in the TEXTOR plasma with injections of neon [5,6], whereas larger plasma machines (like JET, JT-60, or ASDEX Upgrade), with their higher plasma edge temperatures, require a stronger radiator such as Ar or Fe [7,8]. Still larger future machines (of the ITER class) may need an even heavier impurity such as Kr [9]. Indeed, some of the radiative properties of krypton for use on ITER have already been investigated on the TFTR tokamak [10,11], where it was found that most radiation is likely to come from the cooler edge region of the plasma. Recently, the radiative cooling coefficient for Kr in a magnetically confined fusion plasma has been computed [12]; the highest cooling rate results from the open M-shell Kr ions that we observe in the present work. These M-shell ions achieve their equilibria at temperatures from 100 eV to a few hundred eV [12]; these are the temperatures in the crucial outer region of the plasma from just inside the last closed magnetic flux surface out to the plasma's edge. The present observations of the soft-x-ray spectra from nearly all M-shell Kr ions are crucial for understanding the radiative pattern of candidate elements for radiative-mantle scenarios. Interest in extreme ultraviolet (EUV) spectra of krypton also arises in the field of the interaction of high intensity laser pulses with atomic clusters [13], where krypton and argon survey spectra were employed to optimize EUV/x-ray pulse generation.

In order to understand the behavior of injected gases in a plasma and to interpret the measured data, one relies heavily on modeling efforts that in turn require reliable atomic data as input. If one searches the databases for spectroscopic data on the various Kr ions, however, one finds that the knowledge is rather poor and incomplete. A recent survey states that for the middle charge states of Kr, Kr^{10+} to Kr^{16+}, no wavelengths are listed at all [14,15]. For many of the adjacent charge states the knowledge is similarly incomplete. Only some of the missing knowledge can be substituted by calculations, since for any detailed diagnostic work based on a comparison with the results of collisional-radiative models, one realizes the need to also calibrate the latter by experimental data.

Designed as a spectroscopic source [16], the electron beam ion trap has been used extensively for x-ray spectroscopy of highly charged ions [17–19]. Recently, the extreme ultraviolet region was opened to high-resolution spectroscopy with the use of grating spectrometers [20], allowing measurements in the 20–200 Å wavelength band. In this source, the ions are practically at rest, and accurate wavelength measurements are feasible without any Doppler shifts. Also, as ionization and excitation proceed in a stepwise fashion, the electron beam energy determines the highest charge state that can be produced. By adjusting that energy, spectral lines of ions of a single charge state can be added to a spectrum that has been recorded at lower energy. Hence systematic work becomes possible that identifies spectral lines by element and production threshold (the ionization potential of the next lower ionization stage). This process is demonstrated here with the soft-x-ray spectrum of Ni- to Al-like ions of Kr ($Z=36$), following our earlier example of Au ($Z=79$) [21] and using the same moderate-resolution apparatus. We note that another electron beam ion trap has been used by Kink *et al.* to study spectra of more highly charged ions of krypton that appear at shorter wavelengths (5–8 Å) [22] than studied here. Those authors employed a microcalorimeter detector that would have yielded a resolving power of only about 50 in our region of interest whereas our spectrometer reaches 500 (see below).

*Also at IPNAS, Université de Liège, B-4000 Liège, Belgium. Permanent address: Fakultät für Physik und Astronomie, Ruhr-Universität Bochum, D-44780 Bochum, Germany.

Calculations in the present work include emission from the $n=3$ to $n'=5$ emission bands in highly charged Kr ions; these bands are non-negligible in their strength and interweave themselves with the $3d$-$4f$ bands in different Kr charge states. They must be taken into account in any spectroscopic survey work, as well as in diagnostic applications (because of incidental line blends involving lines from different charge state ions).

II. EXPERIMENT

The experiment was set up at the EBIT-II electron beam ion trap at Lawrence Livermore National Laboratory. Kr atoms were introduced continuously into the trap via a bleed valve. Typical injection reservoir pressures were in the 10^{-8}–10^{-7} Torr range. However, the pressure inside EBIT remains lower than 10^{-10} Torr. The expanding gas cloud (still at ultrahigh vacuum) crosses the well-collimated and magnetically compressed electron beam that is at the heart of EBIT. Once atoms have become ionized by collisions with the electrons, they are confined axially by the drift tube voltages (a few hundred V) and radially by the combination of an electron beam (space-charge compensation and attractive potential) and 3 T magnetic field (greatly reducing any radial diffusion). Thus the ions are kept in the very volume that is pierced by the electron beam, and they can be ionized over and over again, up to the first charge state that has an ionization energy that exceeds the electron-beam energy. This then defines the highest charge state that can appear in the spectra.

Electron beam energies from 300 eV to 5100 eV were employed, which under steady-state conditions should be sufficient to produce maximum ion charge states up to Be-like Kr^{32+}. In the present study, however, the electron beam ion trap was operated in a cyclic mode with cycle times shorter than required to reach the highest charge states by stepwise ionization. Consequently, the highest charge states identified in our spectra are not higher than Kr^{23+}. The electron beam currents varied from 5 mA at the low energies to 90 mA at the highest ones. Across the electron beam, the electron energy distribution has a width of about 60 eV [18]. The ions were kept inside the trap for about 0.2 s and then the trap was purged. However, as the build-up phase is included in the observation, the spectrum comprises not only ions of the final charge state distribution (observed under quasi-steady-state conditions for most of the cycle), but also lower charge state ions from the initial transient phase.

The light from the trapped ion cloud was observed by a flat-field spectrometer [23] equipped with a variable-line-spacing grating having a 2400l/mm central line density and a cryogenically cooled, thinned, back-illuminated charge-coupled device (CCD) multichannel detector. The detector has 1024×1024 pixels of 24 μm pixel size. Along the spectrum 950 channels were evaluated, while across the dispersion direction the spectra—after filtering for cosmic ray events—were binned in a central strip least suffering from the slight line curvature inherent in the flat-field design and then calibrated and analyzed. Specific background spectra were used to determine the background shape (which originates from a combination of CCD, read-out noise, thermal noise, and a possible true background continuum) under the data, and to subtract this background from the spectra. Background spectra were sampled both with the Kr injection switched off and with an inverted trap, that is, a trap with inverted drift tube voltages so that ions would be driven out of the trap volume [24]. Typical observation times were 20 min per exposure. This is a compromise of long exposure times wanted for a good signal-to-noise ratio on one hand and the need to be able to recognize cosmic ray events and correct for them on the other; with too many such events in an exposure the filtering process may be less successful. Repeat exposures at various electron beam energies ascertained the general reproducibility of the spectral features and their relative intensities. Four such exposures each were added for the spectra shown in this work.

The spectra were recorded from about 20–75 Å in a single exposure. They were calibrated with the well-known $1s$-$2p$ transitions in H-like ions and $1s^2$-$1s2p$ and $1s^2$-$1s3p$ transitions in He-like ions of C(33.736,40.268,34.973 Å), N(24.781,28.787,24.898 Å), and O(18.969,21.602,18.627 Å) [25]. Each of these is known to be better than 1 mÅ. These lines were produced in dedicated spectra (without Kr ion injection) at lower electron energies. The C, N, and O lines also showed as background in some of the Kr spectra. The dispersion was calculated using a third-order polynomial fit to the calibration lines. The wavelength calibration is better than 0.05 Å in the wavelength interval 20–40 Å. Beyond 40 Å, the wavelength scale to first order has to rely on an extrapolation and consequently is less precise (although the trend of the dispersion is known from various other measurements). Fortunately two transitions of Kr are known that complement the above calibration by providing internal reference data. These are the $3d$-$4f$ transitions of Ni-like Kr^{8+} (75.445,76.296,76.789 Å [26]) and K-like Kr^{17+} (35.190,35.397 Å [25,27]). The former confirms our above calibration and extends it to the upper end of our observation range, while the latter registers as a rather clean line in the middle of our spectra, and thus also in the range of the light-ion reference lines.

However, the long-wavelength end calibration point is not without problems. There are three Kr^{8+} lines near 75 Å that represent $3d^{10}$-$3d^9 4f$ $J=0$–$J'=1$ transitions [28]. Of these, the strongest line, with the shortest wavelength, arises from the decay of the $^1P_1$ level. The calculation (see below) predicts $3d^{10}$-$3d^9 5p$ $J=0$–$J'=1$ transitions with lines in about the same position, and with line intensities that are intermediate to those of the $3d$-$4f$ transitions. All this combined prevents us from calling this line appearance a definite proof of identity with the $3d^{10}\,{}^1S_0$–$3d^9 4f\,{}^1P_1$ transition. Similarly, the purported $3d$-$4f$ transitions in the K-like ion have been identified with the above lines near 35 Å only in an earlier, printed edition of the Kelly tables [25] and are listed in the Shirai tables [14,15], but do not any longer appear in the much later on-line version of the Kelly tables [29]. Our new data corroborate the earlier assignment.

Unfortunately, our spectrometer cannot resolve the fine structure of either line group, which limits the precision of the wavelength scale. Also, many of the strong lines in the

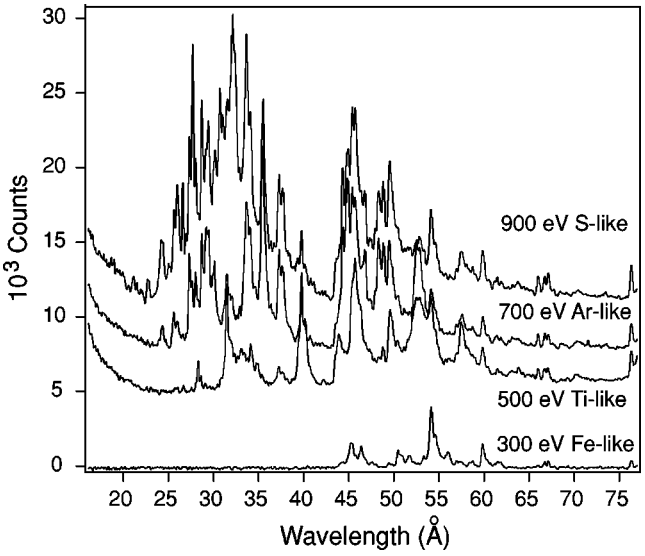

FIG. 1. Sample spectra of Kr in the wavelength range 20–75 Å. The spectra are displaced vertically by arbitrary offsets. The electron beam energies are indicated. Labels indicate the highest-charge state component (by isoelectronic sequence) expected to be produced. In the lowest electron energy spectra, some of the spectral features arise from charge states lower than Ni-like Kr, for which no calculations are available presently.

Kr spectra are blended with others, so that most of the individual line positions cannot be determined with the same precision as possible for single lines. By virtue of the spectrometer geometry, linewidths varied across the spectral range, but generally were about 0.08 to 0.06 Å (full width at half maximum), which is not much more than the interval corresponding to the width of each CCD pixel. Examples of our spectra are shown in Fig. 1.

The reproducibility of the line positions from exposures at one electron-beam energy setting to the next was usually better than 0.05 Å. In some series of spectra, line positions differ by one such step (one pixel size), which may relate to thermal and/or vibrational instabilities of the spectroscopic setup and thermal gradients across the CCD chip. As the linewidth was rather close to a single pixel width, the 25 μm pixel size also posed a limit to spectral analysis.

III. CALCULATIONS

The calculations for Kr in the present work follow the example of calculations for W and Au that have recently been published elsewhere [21,30], which use a Maxwellian electron energy distribution to mimic the temperature in a plasma device. The present calculations corroborate that most lines in our spectral range from the charge states of interest (Ni- to Al-like) appear in a systematic progression of lines from 76 Å (Ni-like, known as $3d$-$4f$ lines) via 36 Å (known $3d$-$4f$ transitions in K-like Kr^{17+}) to about 33 Å (Ar-like Kr^{18+}). In the same ions, $3d$-$4p$ lines are expected at somewhat longer wavelengths and at lower intensities due to the lower statistical weights and the change of angular momentum against the preferred direction of lower l. Ions in higher-charge states (without $3d$ electrons in the ground configurations) may be expected to show $3p$-$4d$ transitions in the wavelength range below 34 Å. For example, the $3p$-$4d$ lines in Kr^{18+} are expected at 27.8 and 28.5 Å. However, there are also metastable levels with a $3p$ hole and a $3d$ electron in these more highly charged ions, which give rise to notable $3d$-$4f$ lines. Each Kr ion with $3d$ electrons in its ground configuration has strong emission features from bands of $3d$-5ℓ, $\ell=f,p$, transitions at larger transition energies than for the corresponding $3d$-$4f$ arrays. In the superposition of emission from all the present Kr ions, the $3d$-5ℓ transition arrays from lower-charge states interweave with the $3d$-$4f$ bands in more highly charged ions. At the lower electron beam energies, spectral features are present that have not been modeled here and that probably arise from lower-charge state ions than Kr^{8+}.

Synthetic collisional-radiative spectra have been computed for Kr^{8+} to Kr^{23+}. The atomic data used to simulate the spectra have been generated with the HULLAC suite of codes [31–33]. Energy levels and $E1$, $E2$, $M1$, and $M2$ transition rates are computed with the fully relativistic parametric potential code RELAC [32]. Cross sections for the electron impact excitation of bound electrons are computed semirelativistically in the distorted-wave approximation (DWA) [33]. The distorted-wave cross sections are integrated over a Maxwellian distribution of free electron energies to determine the final impact excitation rate coefficients. The electron impact excitation rate coefficients and the radiative transition probabilities are then entered into the collisional-radiative rate matrix. The relative populations for the levels of each ion are found in steady state by solving the coupled set of rate equations:

$$n_j\left\{\sum_{i<j}^{M}(A_{ji}+N_eQ_{ji}^d)+\sum_{k>j}^{M}N_eQ_{jk}^e\right\}=\sum_{k>j}^{M}n_k(A_{kj}+N_eQ_{kj}^d)+\sum_{i<j}^{M}n_iN_eQ_{ij}^e, \quad (1)$$

where n_j is the relative population of level j, Q_{ji} is the collisional rate coefficient from level j to level i for excitation (e) or deexcitation (d), A_{ji} is the radiative transition probability from level j to level i, and M is the number of levels used in the model for that ion. The results of these calculations are summarized in Fig. 2.

All electric and magnetic dipole and quadrupole radiative transitions ($E1$, $M1$, $E2$, and $M2$) as computed by RELAC are taken into account. Due to computational difficulties, the $3p$-$4d$ transition arrays have not been included in the Cr-, V-, Ti-, and Sc-like models. This seemed justified, because in the spectra of Ni- to Mn-like ions as well as Ca-like ions, the corresponding lines are seen to be negligible. The results of these calculations for the 3-4 and some 3-5 transitions are summarized in Fig. 2. For clarification of the interpretation, we show the calculated spectrum of Ca-like Kr^{16+} in Fig. 3. In both Figs. 2 and 3, the calculated line emissivity for each transition has been convolved with a Gaussian profile of

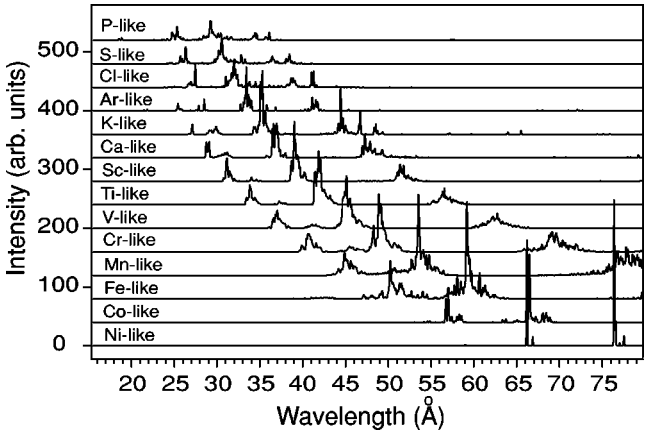

FIG. 2. Collisional-radiative synthetic spectra for Ni-like Kr^{8+} to P-like Kr^{21+}. Not all spectra have been calculated with the same level of completeness. For example, the synthetic spectra for Mn-like to Sc-like ions lack the (weak) $3p$-$4d$ transition array.

100 mÅ full width at half maximum; at this resolution, individual lines are blended into unresolved features for each transition array.

The narrow strong line group in Fig. 3 below 30 Å is from the $3d$-$5f$ transition array, and the next triangular spectral shape just above 30 Å is from the $3d$-$5p$ array. There is a weak background under both the $3d$-$5f$ and $3d$-$5p$ bands that is composed of the $3p$-$4d$ transitions. The strong lines near 37 Å represent $3d$-$4f$, with very weak $3p$-$4s$ lines underneath. The wider line group in the range 48–52 Å is mainly from $3d$-$4p$ transitions. In every case, there are multiple transition arrays for each class of transitions. For example, for the $3d$-$4p$ transitions, there is the dominant $3p^6 3d^2$-$3p^6 3d 4p$ array, and there are weaker satellite transitions from the $3p^5 3d^3$-$3p^5 3d^2 4p$ array.

The synthetic spectrum of each ion was also computed by integrating the DWA collision cross sections, assuming an electron beam with a Gaussian energy distribution of mean energy equal to typical beam energies used in the experiment and with a full width at half maximum of 60 eV. The relative strengths of the emission features in each ion are found to be nearly the same in the two simulations. The predicted relative intensities of each ion's spectral features are used in making line identifications. Our model underlying the collisional-radiative spectrum accounts for dipole-forbidden radiative channels and collisional depopulation of long-lived levels. (Collisional destruction of the ground and excited levels in each ion through electron impact ionization has been neglected in these models.) The present calculations aim at providing a guideline to the identity and wavelengths of the strongest (expected) lines of each ion and estimates of relative intensities of neighboring lines.

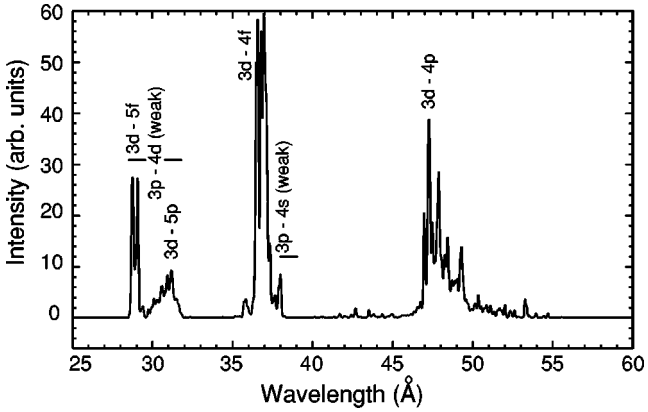

FIG. 3. Calculated spectrum of Ca-like Kr^{16+} with identifications of the major features.

IV. DATA AND DISCUSSION

The spectra (Fig. 1) have a few striking features that can be discussed before considering details. Towards short wavelengths, there is a rising background that remains after the subtraction of the CCD-intrinsic background, and which can be established with spectra under inverted-trap conditions or with the electron-beam off. The spectra also show a gap near 45 Å. It can be attributed to the efficiency curve [34,35] of the diffraction grating and CCD camera, which shows a ''carbon gap,'' as discussed below. This gap has been taken into account in the line identifications.

Data were recorded at electron beam energy settings of 300 eV (Fe-like), 500 eV (Sc-like), 700 eV (Ar-like), 900 eV (P-like), 1000 eV (Si-like), 1100 eV (Mg-like), 1200 eV (Na-like), 1300 eV (Ne-like), 1600 eV (Ne-like), 3000 eV (F-like), 3900 eV (Be-like), and 5100 eV (He-like) (energies without correction for the space charge; the highest expected charge state, identified by the isoelectronic sequence, is given in parentheses). At the lowest electron beam energy setting, spectral structures apparently from ions up to at least Kr^{10+} are present, which complies with expectation. At the next electron energy, 200 eV higher, about four more charge states are expected to contribute, and so on. Exceeding the production threshold of a given ion, however, does not imply that a spectral line from the newly reached charge state appears brightly enough to be recognized. Optimum production regularly happens at energies some 15–20 % above threshold, and such electron energies are often above the production thresholds of one or more of the higher charge states. This complicates the analysis because lines that become prominent with increasing electron beam energy do not necessarily result from the highest charge state that may be reached ''in principle,'' but often refer to ions of one or more charge states down. Only lines from ions in charge states that require higher production energies can be positively excluded, which is helpful. The $n=3$ shell is exhausted above 1.2 keV, so the highest electron beam energy spectra of our sample just proves that the lower-charge spectra persist, because in each cycle the ions are produced afresh, sequentially from neutral gas.

The spectra show a progression of bandlike features, with a few linelike features on top. The observations confirm the general pattern of the predicted spectra. Very few individual features as narrow as individual lines would be expected (and appear in the calibration spectra). The calculations are not able to predict the observed intensity pattern, because that is affected by the grating properties (see below). Never-

theless, it is straightforward to assign charge states of krypton ions to the prominent line groups above 35 Å, and thus also point to $3d$-$4f$ transitions as the major constituents of most of the features that are discernible in our spectra.

Most of the bands are close to positions predicted for $3d$-$4f$ transitions in K- to Ni-like ions. However, both, theory predicts and experiment observes a multitude of additional line clusters. The progression converges near 34 Å, but at higher electron beam energies the line groups of $3p$-$4d$ transitions in the Ar- to Al-like ions (which feature no $3d$ electrons in their ground configurations) are expected to contribute to the spectrum and extend to about 22 Å. The other lines are mostly parts of line clusters, with experiment showing envelopes that differ from the predictions, likely because of different line positions and spacings inside the clusters. Most of these lines are more densely packed than our spectrometer can resolve. For this reason we can give only few individual line wavelengths and mostly discuss partly resolved line groups.

The individual wavelength predictions are good to about ± 0.5Å, or about 1% of the transition energies. The calculations systematically overestimate the transition energy. This is to be expected, since according to the Ritz principle, any imperfect wave function will result in a calculated level energy that is above the true one, and the lowest levels are those that can be calculated best. A seeming exception from the systematic shift of calculated results versus observed wavelengths is the $3d$-$4f$ transition in Kr^{8+}, the wavelength prediction is on the long-wavelength side of the line position given in the literature [25,26,28,29]. However, there is a line near 66.0 Å that would match—by the spacing from the $3d$-$4f$ lines—the predicted wavelength of the $3d$-$5f$ lines, and thus it would corroborate the line identification. Whether this longer-wavelength prediction in the case of Kr^{8+} is an artifact of the calculation, indicates a misidentification of the line given in the literature, or whether it reduces to a calibration problem at the border of the camera chip remains an open question right now.

TABLE I. Lists of prominent lines and suggested identifications based on observed production thresholds and our calculations (see Figs. 1 and 2). Many of the spectral features have been fitted with a higher wavelength precision than is reflected in the number of significant figures given in the table. However, because most of the spectral peaks suffer from spectral blends, the numerical precision does not carry similarly accurate spectroscopic information. In order to preempt confusion, we elected to present rounded off wavelength data.

Wavelength observed (Å)	Comment	Kr spectrum	Transition	Wavelength observed (Å)	Comment	Kr spectrum	Transition
21.2				37.1		XVII	$3d$-$4f$
21.8				37.5		XIV	$3d$-$5f$
22.6				39.6		XVI	$3d$-$4f$
	22.743 [27,37]	XXVI	$3p$-$4d$	≈40.7		XIII	$3d$-$5f$
23.3				≈42.0	Expected	XV	$3d$-$4f$
23.8				≈44.3		XII	$3d$-$5f$
24.1				45.2	45.5 XIII [37]	XIV	$3d$-$4f$
24.6				45.7			
25.0		XXII	$3p$-$4d$	46.2			
25.4		XXII	$3p$-$4d$	46.7			
25.7				47.2			
26.0		XIX	$3d$-$5f$	48.2			
		XXI	$3p$-$4d$	48.8		XIII	$3d$-$4f$
26.4		XXII	$3p$-$4d$	49.5	49.5 XII[37]	XIII	$3d$-$4f$
27.1		XVIII	$3d$-$5f$	50.4		XI	$3d$-$5f$
27.5		XX	$3p$-$4d$	51.6			
27.9		XIX	$3p$-$4d$	≈52.0		XI	$3d$-$5f$
28.5		XXII	$3d$-$4f$	52.9			
28.9		XVII	$3d$-$5f$	54.1	53.5 XI [37]	XII	$3d$-$4f$
29.3		XVII	$3d$-$5f$	57.1			
29.8		XXI	$3d$-$4f$	57.6		X	$3d$-$5f$
30.6		XX	$3p$-$4d$	58.6			
31.2		XVI	$3d$-$5f$	60.0		XI	$3d$-$4f$
31.7				61.4			
32.5		XX	$3d$-$4f$	61.9			
33.4		XIX	$3d$-$4f$	64.0			
33.9		XV	$3d$-$5f$	66.1		IX	$3d$-$5f$
35.3	35.190 [14]	XVIII	$3d$-$4f$	66.9		X	$3d$-$4f$
	35.397 [14]	XVIII	$3d$-$4f$	67.1		X	$3d$-$4f$
	≈35.6 Expected	XVIII	$3d$-$4f$		75.455 [14]	IX	$3d$-$4f$

For the other $3d-4f$ transitions, the difference of predicted and observed wavelengths is almost constant, from 0.5 Å for Kr^{9+} to about 0.7 Å for $Kr^{15+,16+}$. A peculiarity is apparent for the same transition array in the Ti-like Kr^{14+} ion, as no prominent line feature shows in our spectra at or near its predicted wavelength of 42 Å. The explanation is suggested by the overall shape of our Kr spectra, displaying a sawtooth shape with a minimum near 40–42 Å and a maximum near 45 to 50 Å. This is caused by the carbon *K* absorption edge, that is, absorption by a carbon or carbohydrate layer contaminating the surface of the diffraction grating and/or the cryocooled face of the CCD detector chip. The carbon *K* absorption edge can be seen permanently in response measurements of one of our spectrometers at the Advanced Light Source [34,35]. Such absorption by a carbon layer on the camera chip has also been found elsewhere [36]. This absorption feature in the efficiency curve can also explain the relatively weak appearance of the $3d-4f$ transitions in the Sc-like ion Kr^{15+} near 39.6 Å (and the almost missing $3d$-$5f$ array from the Cr-like ion in between).

On the other hand, there are also prominent spectral features that are not predicted by our calculations. For example, near 52.9 Å, a fairly bright line appears in the spectrum recorded at an electron beam energy of 500 eV and persists much more weakly in the spectra recorded at higher electron energies. This line is clearly not identical with the $3d$-$5f$ transitions in Fe-like Kr^{10+} that appear at slightly shorter wavelengths. In the same spectrum, lines show at 39.6 Å (much more strongly than the aforementioned $3d$-$4f$ transition in Kr^{15+} as apparent at higher electron energies, and close to, but resolved from, one of our calibration lines in carbon) and at 31.7 Å.

We find sufficient regularities in our spectra to suggest identifications for $3d$-$4f$ line groups ranging from Kr IX to Kr XXI, for $3d$-$5f$ line groups from Kr IX to Kr XVIII, and for $3p$-$4d$ line groups in the spectra Kr XIX to Kr XXII. The 3-4 transition arrays in Si-like Kr XXIII and Al-like Kr XXIV were also calculated and indicate prominent lines near 24 and 28 Å for the former and near 23 and 27 Å for the latter. We have seen a number of lines in these ranges that would be in reasonable agreement with the calculated wavelengths. However, a more detailed study would be required to ascertain any such identifications near the end of the charge state distribution reached in this experiment, preferably as part of an isoelectronic study to be done with an instrument that permits a higher spectral resolution. The wavelength coincidence of one of our short-wavelength lines with the strongest component of the $3p$-$4d$ multiplet in Kr XXVI (Na-like ion) may be fortuitous, and cannot be taken as a proof of production of this high-charge state.

Our line identifications are presented in Table I and Fig. 4. Many of the spectral features have been fitted with a higher wavelength precision than is reflected in the number of significant figures given in the table. However, because most of the spectral peaks suffer from spectral blends, the numerical precision does not carry similarly accurate spectroscopic information. In order to preempt confusion, we elected to present rounded off wavelength data.

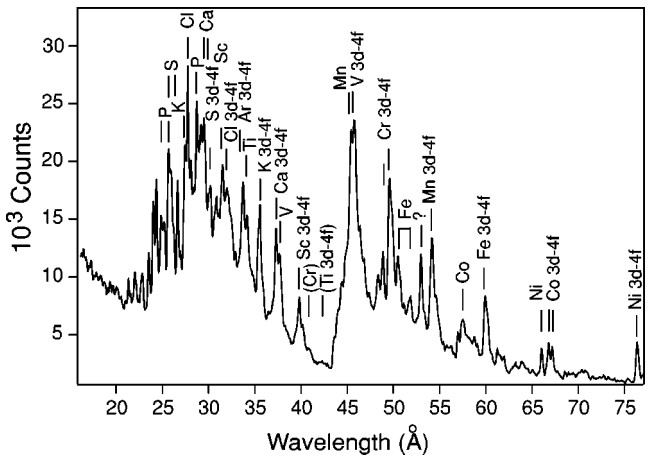

FIG. 4. Spectrum of Kr from the same series as those presented in Fig. 1. Prominent spectral features associated with $3d$-$4f$ transitions are labeled by the isoelectronic sequence. The missing $3d$-$4f$ lines from the Ti-like Kr ion coincide with the carbon *K* absorption edge, which diminishes the response of our spectrometer for wavelengths at and below this edge. Isoelectronic sequence labels without a transition label refer to $3p$-$4d$ and $3d$-$5f$ transitions. This spectrum has been recorded at a higher electron beam energy (5 keV) than those in Fig. 1. Consequently, the high-charge state lines below 35 Å are more prominent. However, the cycle time was too short to achieve steady-state conditions.

Wavelength uncertainties are lowest (<0.1 Å) for the short-wavelength part of our spectra, because it is here that we have suitable reference lines. Unfortunately, in this range the line density is too high to identify individual spectral features, and practically all peaks represent unresolved blends. In the middle of our spectral range, we estimate our wavelength uncertainty to be about 0.2 Å, while in the long-wavelength part, with a lack of reference lines and the aforementioned identification problem with Kr IX, the assumed uncertainty is of order 0.5 Å.

We note that Kelly [29] lists five lines in our wavelength range with charge states, but otherwise without classification. While we do not see the lines listed there at 63.5 Å and 71.0 Å, we have lines that roughly match the listed wavelengths of 45.5, 49.5, and 53.5 Å. However, our identifications place each of these lines with an ion charge state that is higher by one unit than that indicated by Kelly (original data by Bleach [37]). Decades ago, Kim [38] suggested three lines at 77.9, 67.0, and 62.2 Å as originating from the Kr IX $3d$-nf ($n=4,5,6$) transitions, but no spectra were shown then to demonstrate the quality of the data. Of these lines, the 67.0 Å line is not far from our assignment, while the first line is out of our range, and the third one not seen here.

Typical plasma spectra so far have a poorer resolution than ours and therefore show even wider features that result from superpositions of several lines each [37,39,40]. In this sense, our data, as limited in spectral resolution as they are, provide significant stepping stones towards the understanding of present plasma spectra as well as towards detail studies of the EUV spectrum of krypton. While regularities permit us to identify the most prominent spectral features with a progression of $3d$-$4f$ transitions, the data demonstrate that

the progression of $3d$-$5f$ transition arrays interferes with the former.

ACKNOWLEDGMENTS

S. B. Utter and K. L. Wong are acknowledged for their help with the data acquisition. E.T. gratefully acknowledges travel support by the German Research Association (DFG) and support by the Belgian FNRS and the Canadian NSERC (via the University of Alberta–Edmonton), as well as the friendly hospitality of the LLNL EBIT group. This project was performed under the auspices of the U.S. Department of Energy by the University of California, Lawrence Livermore National Laboratory, under Contract No. W-7405-Eng-48.

[1] S.A. Cohen, K.A. Werly, D.E. Post, B.J. Braams, J.L. Perkins, and D. Pearlstein, J. Nucl. Mater. **176-177**, 909 (1990).
[2] Y. Shimomura, Nucl. Fusion **17**, 626 (1977).
[3] D.E. Post, J. Nucl. Mater. **222**, 143 (1995).
[4] R. Stambaugh *et al.*, Nucl. Fusion **39**, 2391 (1999).
[5] U. Samm, G. Bertschinger, P. Bogen, J.D. Hey, E. Hintz, L. Könen, Y.T. Lie, A. Pospieszczyk, D. Rusbüldt, R.P. Schorn, B. Schweer, M. Tokar, and B. Unterberg, Plasma Phys. Controlled Fusion **35**, B167 (1993).
[6] P.E. Vandenplas, A.M. Messiaen, J.P.H.E. Ongena, U. Samm, and B. Unterberg, J. Plasma Phys. **59**, 587 (1998).
[7] J. Mandrekas and W.M. Stacey, Nucl. Fusion **35**, 843 (1995).
[8] J. Ongena *et al.*, Phys. Plasmas **8**, 2188 (2001).
[9] J. Mandrekas, W.M. Stacey, and F.A. Kelly, Contrib. Plasma Phys. **2-3**, 245 (1996).
[10] M. Bitter, H. Hsuan, C. Bush, S. Cohen, C.J. Cummings, B. Grek, K. Hill, J. Schivell, M. Zarnstorff, P. Beiersdorfer, A. Osterheld, A. Smith, and B. Fraenkel, Phys. Rev. Lett. **71**, 1007 (1993).
[11] M. Bitter, H. Hsuan, K. Hill, R. Hulse, M. Zarnstorff, and P. Beiersdorfer, in *Atomic and Plasma-Material Interaction Processes in Controlled Thermonuclear Fusion*, edited by R.K. Janev and H.W. Drawin (Elsevier, New York, 1993), Vol. 119.
[12] K.B. Fournier, M.J. May, D. Pacella, M. Finkenthal, B.C. Gregory, and W.H. Goldstein, Nucl. Fusion **40**, 847 (2000).
[13] E. Parra, I. Alexeev, J. Fan, K.Y. Kim, S.J. McNaught, and H.M. Milchberg, Phys. Rev. E **62**, R5931 (2001).
[14] T. Shirai, K. Okazaki, and J. Sugar, J. Phys. Chem. Ref. Data **24**, 1577 (1995).
[15] T. Shirai, J. Sugar, A. Musgrove, and W.L. Wiese, J. Phys. Chem. Ref. Data Monogr. **8**, 1 (2000).
[16] M.A. Levine, R.E. Marrs, J.R. Henderson, D.A. Knapp, and M.B. Schneider, Phys. Scr., T **T22**, 157 (1988).
[17] P. Beiersdorfer, R. Marrs, J. Henderson, D. Knapp, M. Levine, D. Platt, M. Schneider, D. Vogel, and K. Wong, Rev. Sci. Instrum. **61**, 2338 (1990).
[18] P. Beiersdorfer, Nucl. Instrum. Methods Phys. Res. B, **B56/57**, 1144 (1991).
[19] P. Beiersdorfer, G. Brown, J. Crespo López-Urrutia, V. Decaux, D. Savin, A.J. Smith, G. Stefanelli, K. Widmann, and K. Wong, Hyperfine Interact. **99**, 203 (1996).
[20] P. Beiersdorfer, J. Crespo López-Urrutia, P. Springer, S.B. Utter, and K. Wong, Rev. Sci. Instrum. **70**, 276 (1999).
[21] E. Träbert, P. Beiersdorfer, K.B. Fournier, S.B. Utter, and K.L. Wong, Can. J. Phys. **79**, 153 (2001).
[22] I. Kink, J.M. Laming, E. Takács, J.V. Porto, J.D. Gillaspy, E. Silver, H. Schnopper, S.R. Bandler, M. Barbera, N. Brickhouse, S. Murray, N. Madden, D. Landis, J. Beeman, and E.E. Haller, Phys. Rev. E **63**, 046409 (2001).
[23] S.B. Utter, P. Beiersdorfer, G.V. Brown, E.J. Clothiaux, and N.K. Podder, Rev. Sci. Instrum. **70**, 284 (1999).
[24] H. Chen, P. Beiersdorfer, C.L. Harris, E. Träbert, S.B. Utter, and K.L. Wong, Phys. Scr., T **T92**, 284 (2001).
[25] R.L. Kelly, J. Phys. Chem. Ref. Data **16**, 1 (1987).
[26] J. Reader, N. Acquista, and V. Kaufman, J. Opt. Soc. Am. B **8**, 538 (1991).
[27] J.F. Wyart, TFR Group, Phys. Scr. **31**, 539 (1985).
[28] B.C. Fawcett and A.H. Gabriel, Proc. Phys. Soc. London **84**, 1038 (1964).
[29] R.L. Kelly, on-line data base at http://cfa-www. harvard. edu/amdata/ampdata/kelly/kelly. html
[30] K.B. Fournier, At. Data Nucl. Data Tables **68**, 1 (1998).
[31] A. Bar-Shalom and M. Klapisch, Comput. Phys. Commun. **50**, 375 (1988).
[32] M. Klapisch, J. Schwob, B. Fraenkel, and J. Oreg, J. Opt. Soc. Am. **67**, 148 (1977).
[33] A. Bar-Shalom, M. Klapisch, and J. Oreg, Phys. Rev. A **38**, 1773 (1988).
[34] M. B. Schneider (private communication).
[35] M.J. May *et al.* (private communication).
[36] A. Saemann and K. Eidmann, Rev. Sci. Instrum. **69**, 1949 (1998).
[37] R.D. Bleach, J. Opt. Soc. Am. **70**, 861 (1980).
[38] H.H. Kim, J. Opt. Soc. Am. **58**, 739 (1968).
[39] R.E. Stewart, D.D. Dietrich, R.J. Fortner, and R. Dukart, J. Opt. Soc. Am. B **4**, 396 (1987).
[40] J.L. Weaver, G. Holland, U. Feldman, J.F. Seely, C.M. Brown, V. Serlin, A.V. Deniz, and M. Klapisch, Rev. Sci. Instrum. **72**, 108 (2001).